ACS Medicinal Chemistry Letters

pubs.acs.org/acsmedchemlett
Letter

Quinazolinones as Bioisosteres of Naphthoquinones: A Path to Potent *Hs*DHODH Inhibitors with Optimized Properties

Bruna F. Godoi, Jéssica D. Bueno, Wemenes J. L. Silva, Aline D. da Purificação, Pedro I. P. Leite, Thiago dos Santos, Murillo Freitas, Daniel G. Silva, Tais C. Silva, Josué de Moraes, Caroline S. Freitas, Mayara Mattos, Thiago M. L. Souza, Bianca A. Martin, Renata F. V. Lopez, M. Cristina Nonato,* Carolina H. Andrade,* and Flavio S. Emery*

Cite This: *ACS Med. Chem. Lett.* 2026, 17, 99−108

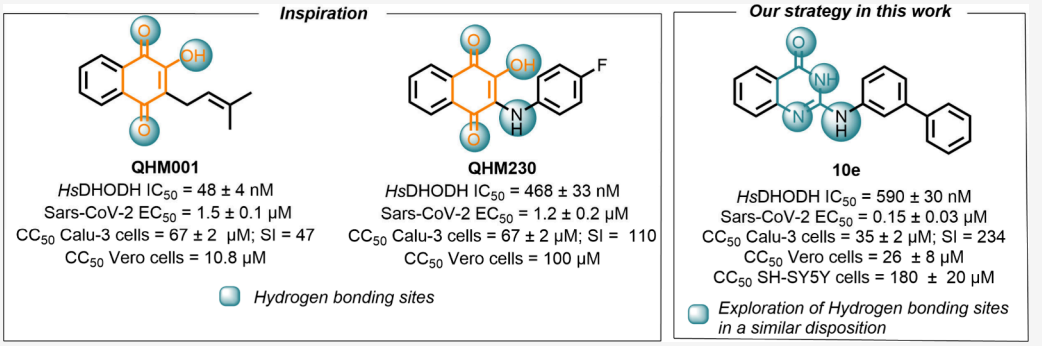

ABSTRACT: Human dihydroorotate dehydrogenase (*Hs*DHODH) is a key enzyme in pyrimidine biosynthesis and a target for antiviral therapies against RNA viruses like SARS-CoV-2. Building on prior quinone-based inhibitors, we explored quinazolinones as bioisosteric replacements to reduce cytotoxicity and off-target effects. Through structure-based design, we synthesized quinazolinone derivatives aimed at maintaining critical binding interactions. First-generation compounds showed moderate *Hs*DHODH inhibition (up to 60% at 250 μM), with compound **10c** having an IC_{50} of 25 μM. Using computational modeling, we optimized second-generation derivatives, with **10e** showing the highest potency (IC_{50} = 0.59 ± 0.03 μM) and significant antiviral activity against SARS-CoV-2 (EC_{50} = 0.15 ± 0.03 μM). These compounds demonstrated improved selectivity compared to naphthoquinone analogs, though challenges with aqueous solubility remain. These results highlight quinazolinones as promising scaffolds for further development of anti-SARS-CoV-2 therapies targeting *Hs*DHODH.

KEYWORDS: *human dihydroorotate dehydrogenase, quinazolinones, host-directed therapy, SBDD, SARS-CoV-2*

The *de novo* synthesis of pyrimidine nucleotides represents a conserved metabolic pathway across bacteria, protozoans, and animals, providing essential building blocks for DNA and RNA biosynthesis.[1] Dihydroorotate dehydrogenase (DHODH) catalyzes the fourth and rate-limiting step in this pathway.[2,3] Located on the outer surface of the inner mitochondrial membrane, human DHODH (*Hs*DHODH) catalyzes the oxidation of dihydroorotate to orotate through a flavin-dependent redox reaction (Figure 1A), which is subsequently utilized for the production of uridine monophosphate (UMP) and downstream pyrimidine nucleotides.[1,4]

Although they are recognized as validated targets for drug discovery, a limited number of *Hs*DHODH inhibitors have reached clinical trials and advanced to the market. For instance, the prodrug leflunomide, metabolized to teriflunomide, is a potent *Hs*DHODH inhibitor that was approved for the treatment of rheumatoid arthritis (Figure 1B).[5−7]

Recent investigations have explored *Hs*DHODH as a target to discover drug candidates for COVID-19.[6,8,9] This metabolic pathway has gained significant attention as a promising target for antiviral therapeutics, as viruses rely extensively on host pyrimidine biosynthesis to support their replication cycles. This host-directed approach offers potential advantages for developing broad-spectrum antivirals with reduced susceptibility to viral resistance mechanisms (Figure 1C).[10−12] Brequinar, originally developed as an anticancer agent,[11] exhibits highly specific and potent inhibitory activity against

Received: April 28, 2025
Revised: August 13, 2025
Accepted: September 8, 2025
Published: September 16, 2025

https://doi.org/10.1021/acsmedchemlett.5c00237
ACS Med. Chem. Lett. 2026, 17, 99−108

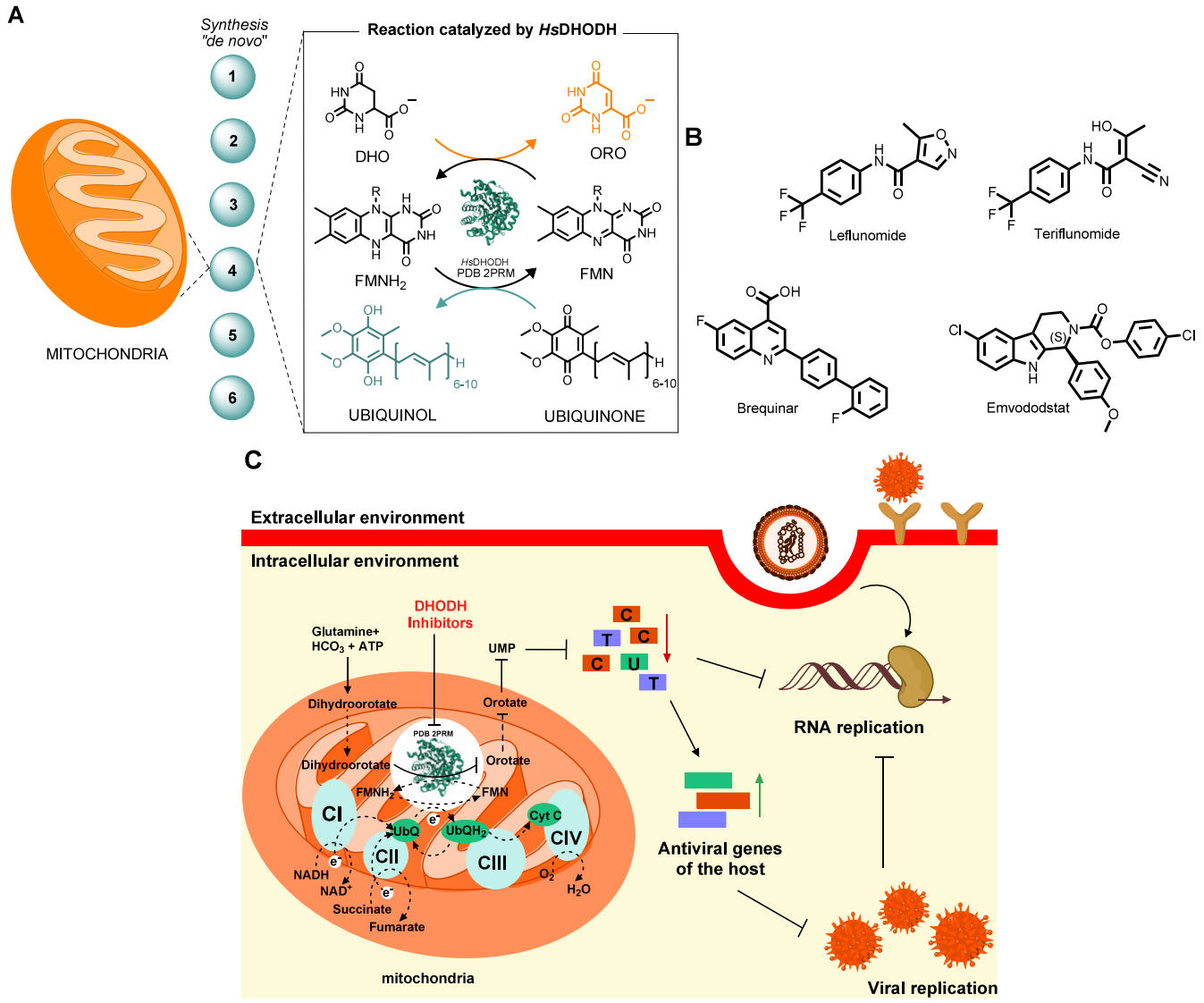

Figure 1. A) Ping-pong mechanism of the fourth step of pyrimidine biosynthesis, performed by the human DHODH. B) Known inhibitors of *Hs*DHODH. C) Strategy of broad-spectrum antivirals through *Hs*DHODH inhibition. The inhibition of DHODH reduces pyrimidine pools, which consequently inhibits RNA replication and activates antiviral genes of the host.

*Hs*DHODH and shows low micromolar anti-SARS-Cov-2 activity (Figure 1B).[13,14]

Emvododstat (PTC299) emerged during the COVID-19 pandemic as a promising drug candidate targeting *Hs*DHODH, demonstrating dual therapeutic mechanisms through direct inhibition of pyrimidine biosynthesis and suppression of pro-inflammatory cytokine production (Figure 1B).[15] Beyond SARS-CoV-2, emvododstat exhibits broad-spectrum antiviral activity against other RNA viruses, including Ebola virus and Hepatitis C virus.[13] Although Phase 2/3 clinical trials for hospitalized COVID-19 patients initially showed encouraging results, these studies were ultimately terminated before completion.[16] The clinical trial failure of *Hs*DHODH inhibitor monotherapy for SARS-CoV-2 is not discouraging the attempts to find clinical candidates targeting this enzyme, as combination therapy with antivirals is a promising approach to fight infections with RNA viruses.[17,18] These preliminary data nonetheless contributed valuable insights regarding the therapeutic potential of inhibiting *Hs*DHODH as a host-directed antiviral drug discovery approach.

In our previous studies, we identified a series of quinone-based compounds as potent inhibitors of *Hs*DHODH (as Lapachol and QHM230, Figure 2A), exhibiting nanomolar IC_{50} values and demonstrating in vitro activity against SARS-CoV-2 in the micromolar range.[19] These findings highlight the therapeutic potential of *Hs*DHODH inhibition as a host-directed antiviral strategy. Molecular docking analyses revealed that these quinoidal inhibitors establish binding interactions similar to Brequinar at the enzyme's ubiquinone binding site. Despite these promising results, the naphthoquinone series displayed significant limitations including high cytotoxicity, poor aqueous solubility, and inherent scaffold liabilities related to promiscuous reactivity and metal chelation.[19−21]

To address these liabilities while maintaining potent inhibitory activity, we hypothesized that replacing the hydroxynaphthoquinone core with isosteric quinazolinone or quinoxalinone scaffolds could enhance drug-like properties while preserving critical binding interactions. In this work, through structure-based drug design (SBDD), we identified and validated quinazolinones as promising bioisosteres of the

https://doi.org/10.1021/acsmedchemlett.5c00237
ACS Med. Chem. Lett. 2026, 17, 99−108

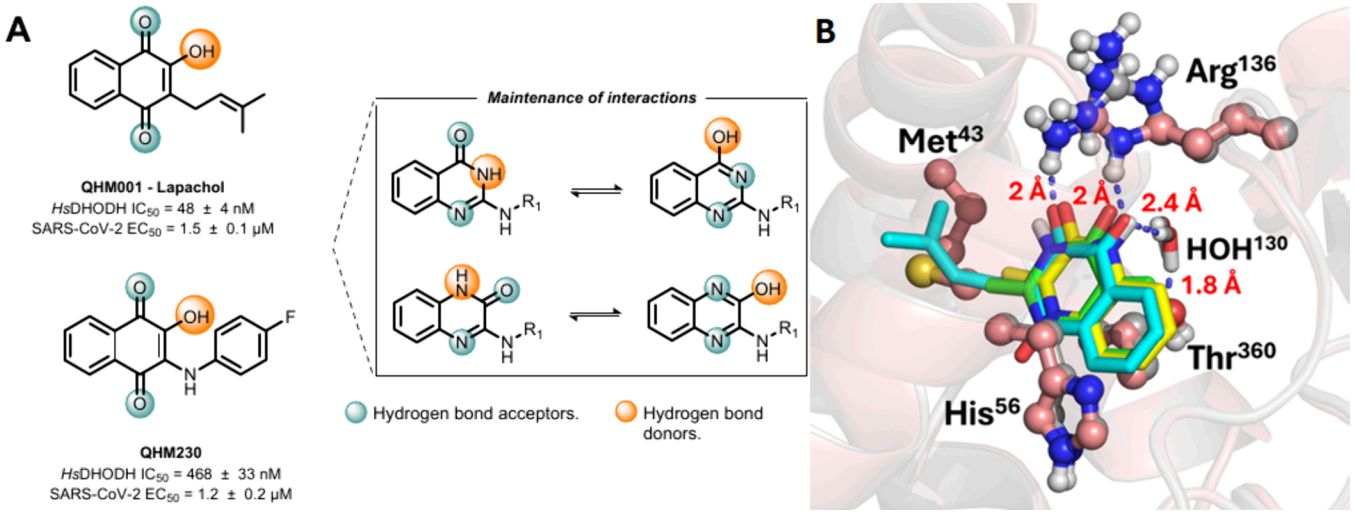

Figure 2. A) Structural conservation of hydrogen bond donor and acceptor groups in quinazolinones and quinoxalinones, compared to the characteristic electronic configuration of napthoquinones described in prior studies (Lapachol and QHM230). B) Structural superposition of the *Hs*DHODH−Lapachol complex in its crystal conformation (PDB ID 9CCC), represented in cyan, with the resulting molecular docking models of the quinazolinones (green) and quinoxalinones (yellow). Docking calculations were performed using the crystal structure PDB ID 6LP6 as a target. Hydrogen bonds between lapachol and residues in the *Hs*DHODH binding site are highlighted in blue dashed lines, and the interatomic distances are indicated.

Scheme 1. Synthetic Routes for the Synthesis of Quinoxalinones (Route A) and Quinazolinones (Route B)[a]

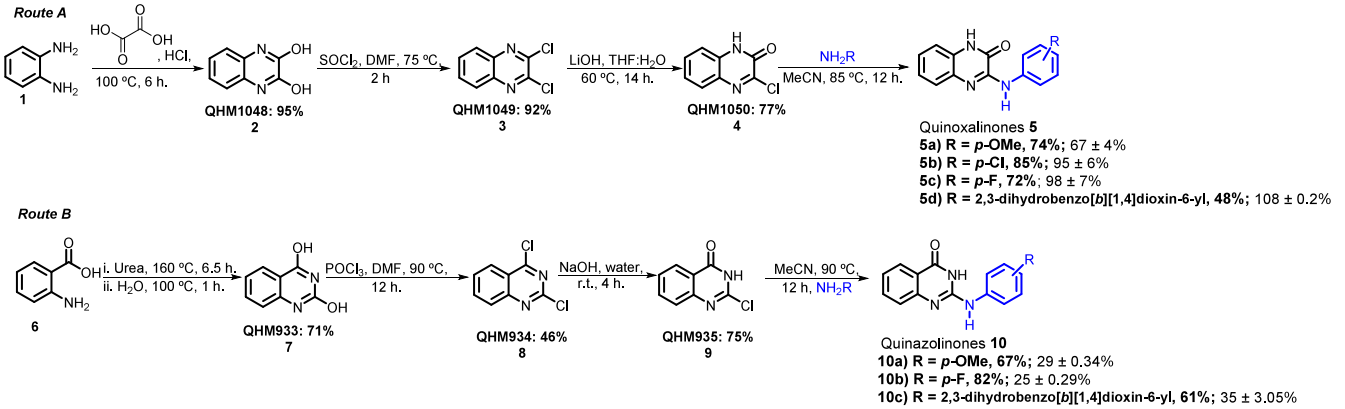

[a]The percentages highlighted in bold show isolated yields of compounds. The percentages in normal font show the enzymatic activity and standard deviation at 250 μM (100% activity = 0% inhibition).

naphthoquinone core. Herein, we report the design, synthesis, molecular interactions, and biological evaluation of novel *Hs*DHODH inhibitors that demonstrate anti-SARS-CoV-2 activity with improved physicochemical and toxicological profiles. Our optimization strategy focused on enhancing both polar and hydrophobic interactions within the enzyme's binding site. In the first screening, we selected matched pairs (such as fluorine and chlorine in the para position, the most potent compounds in the previous paper) in order to compare the inhibitory activity of quinones, quinazolinones, and quinoxalinones. Moreover, since electron-donating groups were not assessed in the past paper, we also added *p*-methoxy and 2,3-dihydrobenzo[*b*][1,4]dioxin-6-yl groups to better understand the SAR.

We established two linear synthetic routes to obtain the designed quinoxalinones (**5a−d**) and quinazolinones (**10a−c**) as depicted in Scheme 1. For quinoxalinones (Route A), we conjugated oxalic acid with 1,2-diaminobenzene under acidic conditions to afford 1,4-dihydroquinoxaline-2,3-dione (**2**) in 95% yield,[22] which was further chlorinated via thionyl chloride to yield 2,3-dichloroquinoxaline (**3**).[23] Selective hydrolysis of **3** using lithium hydroxide yielded 3-chloroquinoxalin-2(1*H*)-one (**4**), which was then reacted with anilines to provide the desired set of 3-amino-substituted quinoxalinones with yields ranging from 48 to 85%.[23,24] For 2-amino-substituted quinazolinones (Route B), we reacted 2-aminobenzoic acid and urea according to Gong and co-workers' procedure[25] to produce quinazoline-2,4-diol (**7**, 71%) on a gram scale. After dichlorination with phosphoryl chloride, selective hydrolysis with sodium hydroxide, and nucleophilic substitution with the respective anilines, we obtained 2-amino-quinazolin-4-(3*H*)-ones with yields ranging from 61 to 82%.[25−28]

Compounds **5a−d** and **10a−c** were evaluated for *Hs*DHODH inhibition in a single-dose assay at 250 μM, with enzymatic inhibition [±SD (%)] reported without preincubation. Notably, while quinazolinones demonstrated significant inhibitory activity under the assay conditions, the quinoxalinone scaffold failed to inhibit the enzyme. The

https://doi.org/10.1021/acsmedchemlett.5c00237
ACS Med. Chem. Lett. 2026, 17, 99−108

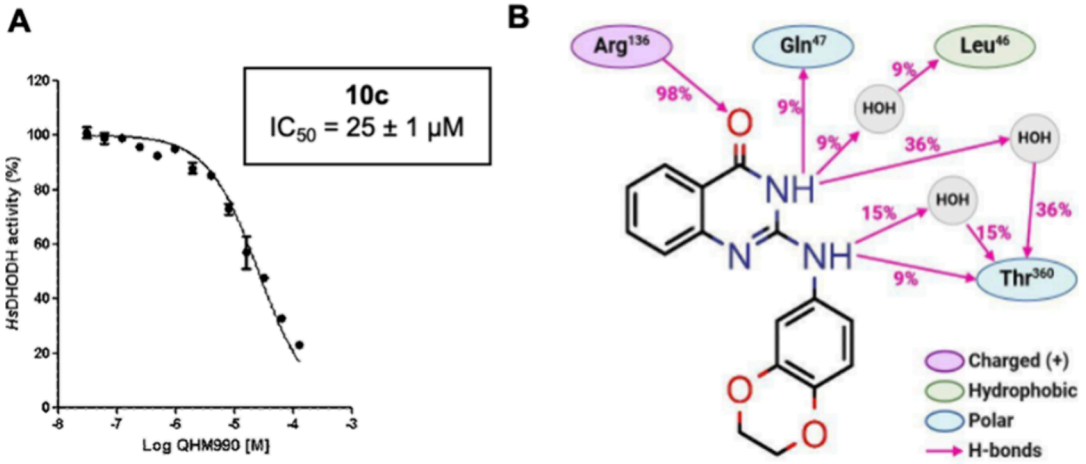

Figure 3. A) **10c** dose−response curve and IC_{50} for *Hs*DHODH inhibition. B) 2D MD analysis, highlighting the relative frequency (%) of molecular interactions between compound **10c** and the enzyme *Hs*DHODH.

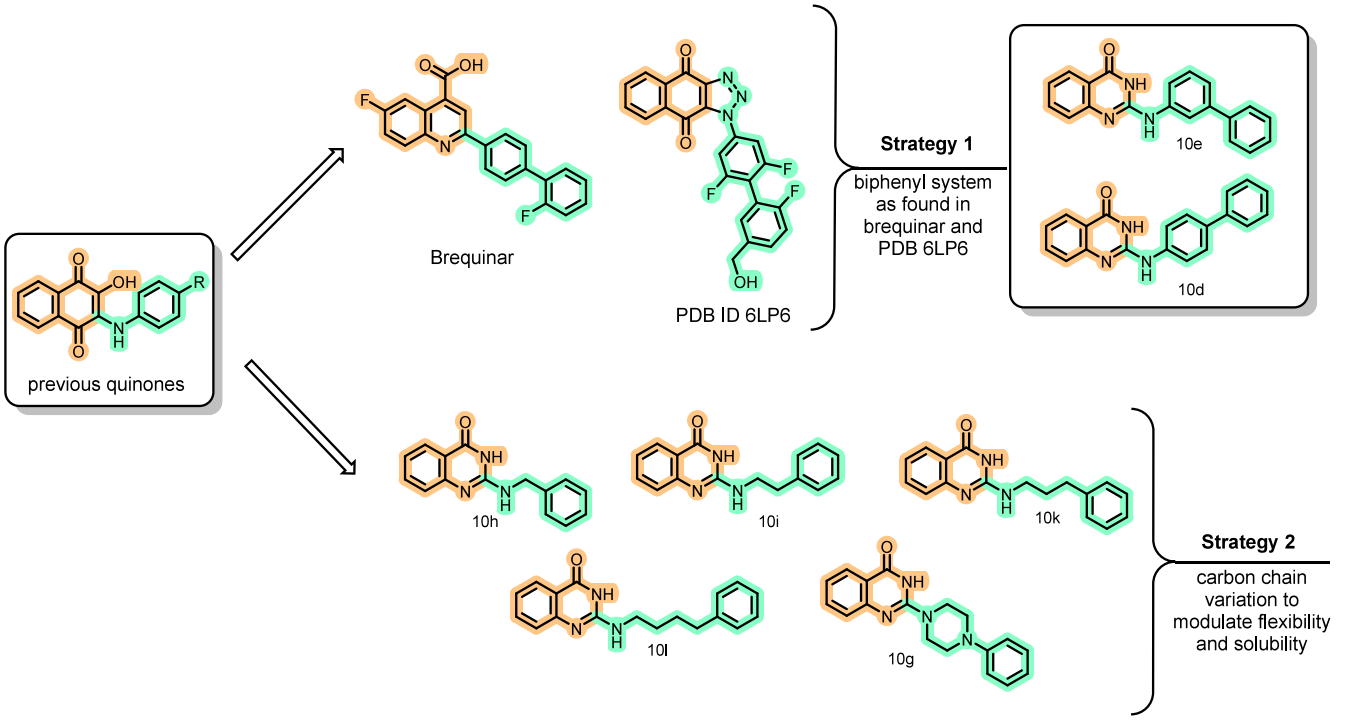

Figure 4. Design of the second generation of compounds. Quinazolinone ring as a bioisostere of naphthoquinone core (highlighted in orange), and two different strategies planned to increase SAR understanding (substitutions highlighted in green).

differences in inhibition profiles can be rationalized by computational analysis revealing suboptimal hydrogen bonding distances between quinoxalinones and the conserved water molecule (3.1 Å, Figure S3) compared to the more favorable interactions observed with Lapachol (2.4 Å) and quinazolinones (2.3 Å, Figure S3). The altered positioning and orientation of the quinoxalinone carbonyl hydrogen bond acceptor, compared to the optimal geometry observed in lapachol (Figure 2B), appears to be a critical factor preventing effective enzyme inhibition, thus failing to mimic the essential interaction pattern established by our previous hits.[19] The quinazolinone derivatives (**10a−c**), however, exhibited promising inhibitory activity, with up to 75% inhibition of *Hs*DHODH in a single-dose assay. Compound **10c** demonstrated dose-dependent inhibition with an IC_{50} value of 25 ± 1 μM. Despite showing higher percent inhibition at the screening conditions, compounds **10a** and **10b** exhibited nonsigmoidal dose−response relationships that precluded reliable IC_{50} determination.

Figure 3A presents the dose−response curve for compound **10c**, calculated IC_{50} for *Hs*DHODH inhibition, and a 2D interaction analysis derived from a 50 ns molecular dynamics (MD) simulation, illustrating the relative frequency (%) of molecular interactions between compound **10c** and *Hs*DHODH. Throughout the MD simulation, **10c** maintained stable binding conformation, as evidenced by a root-mean-square deviation (RMSD) of less than 2 Å (Figure S1A). The analysis reveals a highly conserved hydrogen bond (98% occupancy) between the carbonyl group in **10c** and the side chain of Arg^{136} in *Hs*DHODH (Figure 3B). Additionally,

https://doi.org/10.1021/acsmedchemlett.5c00237
ACS Med. Chem. Lett. 2026, 17, 99−108

Table 1. Experimental Results for Enzymatic Activity at 250 μM, *Hs*DHODH IC_{50}, Cytotoxicity, and Solubility of the Second Generation of Compounds

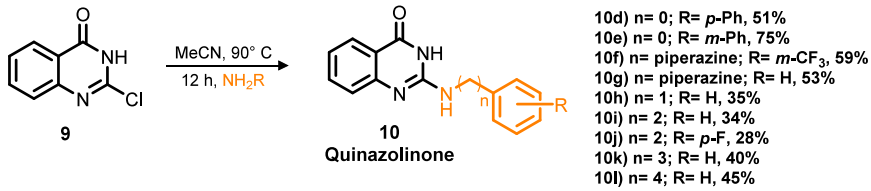

Compound	Enzymatic Activity ± SD (%)	IC_{50} ± SD (μM)	CC_{50} (μM)[a]		Water Solubility (μM)[b]
			Vero Cells	SH-SY5Y Cells	
10c	15.1 ± 0.8	25 ± 1	390 ± 20	100 ± 19	26.0 ± 0.6
10d	49 ± 3	NA[c]	70 ± 10	130 ± 20	n.d.[d]
10e	4.2 ± 0.2	0.59 ± 0.03	26 ± 8	180 ± 20	n.d.[d]
10f	83 ± 7	NA[c]	161 ± 8	200 ± 20	n.d.[d]
10g	126 ± 1	NA[c]	150 ± 20	290 ± 20	n.d.[b]
10h	47 ± 3	NA[c]	50 ± 10	160 ± 20	35 ± 0.5
10i	2.5 ± 0.1	12 ± 1	110 ± 20	140 ± 20	57.0 ± 0.7
10j	8.2 ± 0.4	39 ± 2	40 ± 10	290 ± 30	30 ± 2
10k	18 ± 1	20 ± 1	40 ± 10	290 ± 20	30.0 ± 0.3
10l	34 ± 2	30 ± 2	60 ± 10	200 ± 20	n.d.[d]

[a]Values are expressed as a percentage of the control, and the 50% cytotoxic concentration (CC_{50}) values were calculated based on three experiments using a 95% confidence interval. [b]Water solubility determined using Procedure 2 (SI). [c]NA stands for not applicable, out of the cutoff limit of 70% inhibition. [d]n.d. stands for not determined, out of the detection limit.

transient hydrogen bonds (9% occupancy) were observed between the two N−H groups of **10c** and residues Gln^{47} and Thr^{360}. Water-mediated interactions were also identified, bridging the N−H moieties of **10c** with residues Leu^{46} and Thr^{360}. Notably, this hydrogen-bonding network between **10c** and residues Arg^{136}, Thr^{360}, and Gln^{47} corresponds to interactions previously reported for naphthoquinoidal inhibitors,[19] suggesting a conserved binding mechanism despite the scaffold modification.

Interestingly, during MD analysis, while the benzodihydrodioxine moiety exhibited no observable interactions within the *Hs*DHODH enzyme active site, the 2-aminoquinazolinone core showed multiple interactions (Figure 3B). These observations support our hypothesis that the quinazolinone scaffold effectively mimics the essential binding features of quinones, as demonstrated for lapachol (Figure 2B, PDB: 9CCC). This structural mimicry, coupled with no benzodihydrodioxine-mediated interactions, guided the computational design of a second-generation quinazolinone series to extend binding interactions toward unexplored hydrophobic regions of the enzyme binding pocket. This rational new design focused on enhancing *Hs*DHODH inhibitory potency through strategic optimization of key pharmacophoric elements while improving drug-like properties, particularly aqueous solubility, and preserving structural features critical for target engagement.

To accomplish this goal, we employed computational analysis of **10c**'s binding mode and developed compounds using two distinct optimization strategies (Figure 4):

The first approach was based on structural insights from the potent naphthotriazoledione inhibitor (IC_{50} = 1.2 nM), cocrystallized with *Hs*DHODH (PDB ID: 6LP6),[29] which exhibits interaction patterns analogous to our previously characterized quinone-based inhibitors. The naphthotriazoledione scaffold incorporates a biphenyl ring system that effectively occupies subsite 1, a nomenclature adopted by Baumgartner et al. in 2006[30] (Figure 4). Notably, this biphenyl motif is also present in Brequinar,[31] further validating the significance of this pharmacophoric element in establishing favorable hydrophobic interactions within this region of the binding pocket (Strategy 1 in Figure 4).

The second approach evaluated the importance of an aliphatic linker between the amine −NH and the phenyl substituent to understand whether the added flexibility could improve potency by enabling different interaction patterns (Strategy 2 in Figure 4). Moreover, increasing the sp^3 fraction (Fsp^3) of designed compounds could modulate druglike properties, including solubility.[32] Furthermore, the strategy also contemplates the ability of the series to occupy the hydrophobic subpocket of *Hs*DHODH.

The new designed quinazolinones (**10d−l**) were obtained according to the same synthetic route, and the isolated yields varied from 28 to 75% (Table 1). Table 1 summarizes the enzymatic activity, IC_{50} of the most potent compounds, cytotoxicity in Vero and SH-SY5Y cells, and water solubility. Compound **10c**, the most potent inhibitor from our initial screening, demonstrates substantially lower potency compared to our second-generation compounds, validating our strategic scaffold optimization approach. The enzymatic inhibition data confirm the efficacy of our computational design strategy, with compound **10e** emerging as the most potent inhibitor of this series, exhibiting 96% inhibition of *Hs*DHODH and an IC_{50} of 0.59 ± 0.03 μM at 250 μM (Table 1). The 2D interaction analysis derived from a 50 ns MD simulation of compound **10e** reveals critical binding interactions (Figure 3C). Root mean square deviation (RMSD) analysis demonstrates that **10e** maintains a stable binding conformation throughout the simulation, with minimal positional fluctuations (<1.5 Å) (Figure S2C). In addition to preserving the key interactions with Arg^{136} and the water-mediated hydrogen bond with Thr^{360} observed in **10c**, compound **10e** establishes an additional hydrogen bond between the quinazolinone carbonyl group and Gln^{47}, which contributes significantly to binding stability. Furthermore, a novel water-mediated hydrogen bond

https://doi.org/10.1021/acsmedchemlett.5c00237
ACS Med. Chem. Lett. 2026, 17, 99−108

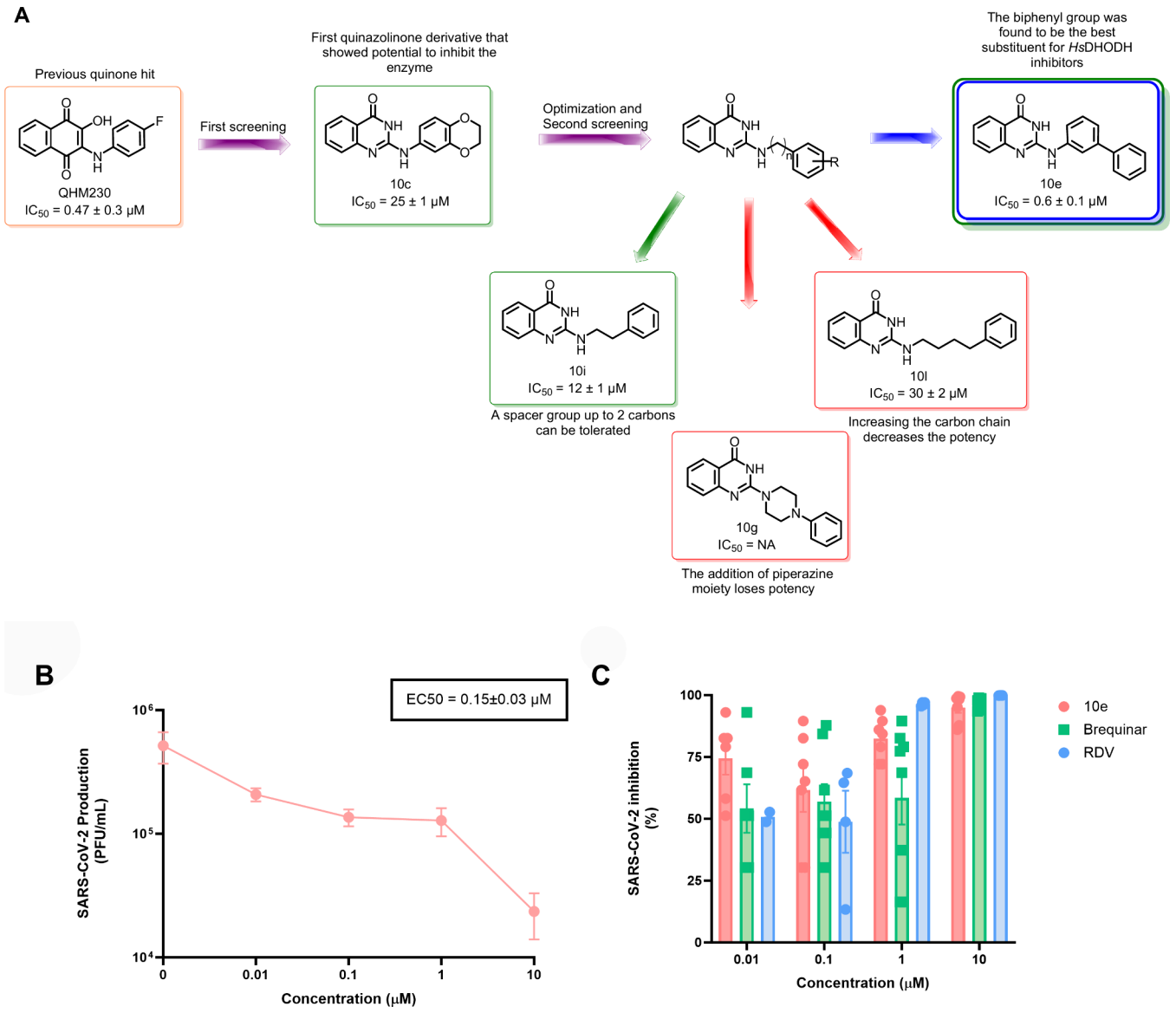

Figure 5. A) SAR diagram summarizing gains and losses of potency for *Hs*DHODH inhibitors. Purple arrows represent the screening. Red arrows represent a decrease in activity. Green arrows represent potency improvement. The blue arrow shows the hit of the work. B) Antiviral activity against SARS-CoV2 in Calu-3 cells of **10e** (orange dot, EC_{50} = 0.15 ± 0.03 μM) and C) percentage of SARS-CoV-2 inhibition, compared with the positive controls Brequinar (green square, EC_{50} = 0.8 ± 0.2 μM) and Remdesivir (blue dot, EC_{50} = 0.030 ± 0.002 μM).

forms between Ala[55] and the N−H from the substituted aniline, providing additional anchoring points within the binding pocket.

More significantly, the enhanced potency of the *m*-substituted **10e** can be attributed to two key $\pi-\pi$ stacking interactions formed between Phe[62], Tyr[38], and the terminal aromatic ring of the biphenyl substituent, interactions that are coherent with those observed in the cocrystal structure of the naphthotriazoledione inhibitor (PDB: 6LP6).[29] The structural features of Brequinar and the tricyclic derivative[29] further corroborate the critical importance of this biphenyl system in establishing optimal contacts with key amino acid residues. The computational prediction of diminished interactions with residues Ala[55] and Tyr[38] can rationalize the substantially reduced potency observed with the *p*-substituted analog.

To analyze the influence of aliphatic spacer groups between the −NH substitution of quinazolinone ring and the phenyl on inhibitory potency, we systematically varied the carbon chain length in a homologous series (**10h−l**). Comparison of compound **10b** (*p*-fluor-aniline, lack of dose−response) with compound **10j** (*p*-fluor-phenethyl-amine), which incorporates an ethylene linker, revealed the latter as a moderate inhibitor, with an IC_{50} of 29 ± 2 μM for **10j**. Interestingly, these results did not align precisely with computational predictions which indicated that a larger spacer group would increase potency. Our experimental results suggest that an ethylene linker represents the optimal substitution pattern. Extension of this linker to three (**10k**) or four (**10l**) methylene units resulted in progressively diminished potency, despite MD analysis predicting a π-stacking interaction between compound **10l** and Phe[62] (Figure S2G,H).

Compounds incorporating the piperazine moiety (**10f** and **10g**) exhibited favorable computational docking scores (Table S1) but demonstrated negligible inhibitory activity against *Hs*DHODH. This discrepancy suggests that the absence of a −N-H hydrogen bond donor at the C-2 position of the

https://doi.org/10.1021/acsmedchemlett.5c00237
ACS Med. Chem. Lett. 2026, 17, 99−108

quinazolinone scaffold is critical for activity. Furthermore, the nonaromatic heterocycle is more rigid that the linear ethylene linker. The loss of this key hydrogen bond donor eliminates essential interactions with active site residues, particularly Ala[55] and Gln[47]. This structure−activity observation underscores the importance of maintaining specific hydrogen bonding capabilities within this region of the inhibitor scaffold for effective target engagement (Figure 5A).

In addition to the enhanced potency observed within our second-generation quinazolinone series, a notable advantage emerged in their improved cytotoxicity profiles compared to our naphthoquinone inhibitors (like Lapachol).[19] Although compounds **10d** and **10e** exhibited moderate cytotoxicity in Vero cell lines, they demonstrated substantially reduced toxicity toward human SH-SY5Y neuroblastoma cells, confirming that the quinazolinone scaffold provides optimized toxicological properties for *Hs*DHODH inhibition (Table 1). However, regarding aqueous solubility, the quinazolinone series did not demonstrate significant improvement compared to the naphthoquinone precursors. Consequently, enhancement of water solubility remains a critical parameter requiring further optimization in subsequent medicinal chemistry efforts.

Following the identification of **10e** as a potent inhibitor of *Hs*DHODH, we evaluated its potential as an antiviral candidate by assessing its cytotoxicity and antiviral activity against SARS-CoV-2 and determining the selectivity index (SI). As shown in Table 2, compound **10e** demonstrates

Table 2. Antiviral Activity against SARS-CoV-2 in Calu-3 Cells of 10e and 10i

Compound	CC_{50} (μM) Calu-3	EC_{50} (μM)	SI
10e	36 ± 2	0.15 ± 0.03	234.7
Brequinar	–	0.8 ± 0.2	–
Remdesivir	–	0.030 ± 0.002	–

potent anti-SARS-CoV-2 activity (EC_{50} = 0.15 ± 0.03 μM) in infected Calu-3 cells, with SI equal to 234, indicating a favorable safety profile. Notably, while **10e** exhibited comparable *Hs*DHODH inhibitory potency to our previously inhibitors,[19] it demonstrated a 10-fold enhancement in antiviral activity compared to lapachol (EC_{50} = 1.5 ± 0.1 μM)—the most potent antiviral quinone in our studies—coupled with significantly reduced cytotoxicity.

Figure 5B and C illustrates the comparative inhibition of SARS-CoV-2 production (PFU/mL) by compounds **10e**, Brequinar (EC_{50} = 0.8 ± 0.2 μM), and Remdesivir (EC_{50} = 0.03 ± 0.0015 μM), the latter two used as positive controls. The results highlight the exceptional antiviral potential of quinazolinone derivative **10e**, demonstrating approximately 5-fold greater potency in suppressing viral replication compared to Brequinar under identical assay conditions and concentrations. This enhanced antiviral efficacy, combined with favorable selectivity indexes, positions this scaffold as promising candidates for further optimization as SARS-CoV-2 inhibitors targeting host pyrimidine biosynthesis.

In conclusion, this study demonstrates the successful design, synthesis, and anti-SARS-CoV-2 evaluation of novel quinazolinone derivatives as potent inhibitors *Hs*DHODH. Employing bioisosteric replacement of the naphthoquinone scaffold, we developed quinazolinones that effectively mimic critical binding interactions within the ubiquinone binding site of the studied enzyme while addressing cytotoxicity and limitations of promiscuous properties inherent to quinone-based inhibitors. Through structure-based design and SAR analysis, we identified **10e** as the most promising compound, exhibiting high *Hs*DHODH inhibition (IC_{50} = 0.59 ± 0.03 μM) and antiviral activity against SARS-CoV-2 (EC_{50} = 0.15 ± 0.03 μM) with a favorable SI (234). MD simulations revealed key determinants of binding affinity, including conserved hydrogen bonding networks with Arg[136], Thr[360], and Gln[47], as well as critical $\pi-\pi$ stacking interactions with Tyr[38] and Phe[62] facilitated by the optimized biphenyl substituent. While our quinazolinone derivatives demonstrate significantly improved potency and reduced cytotoxicity compared to their naphthoquinone counterparts, aqueous solubility remains suboptimal and represents a primary focus for subsequent optimization efforts. Overall, these findings establish quinazolinones as a promising core for *Hs*DHODH inhibition and advance the development of anti-SARS-CoV-2 candidates targeting host pyrimidine biosynthesis.

Safety Statement. No unexpected or unusually high safety hazards were encountered.

■ ASSOCIATED CONTENT

Supporting Information

The Supporting Information is available free of charge at https://pubs.acs.org/doi/10.1021/acsmedchemlett.5c00237.

Tables (docking scores, ligand efficiency, CC50, and solubility), figures (molecular dynamic simulation, docking models, and complex of ligand and *Hs*DHODH), and experimental description (synthetic, biological, and computational procedures and spectroscopic/spectrometric data) (PDF)

■ AUTHOR INFORMATION

Corresponding Authors

M. Cristina Nonato − *Center for the Research and Advancement in Fragments and Molecular Targets (CRAFT), School of Pharmaceutical Sciences at Ribeirao Preto, University of São Paulo, Ribeirão Preto 14040-903 SP, Brazil; Protein Crystallography Laboratory, Department of Biomolecular Sciences, School of Pharmaceutical Sciences at Ribeirao Preto, University of São Paulo, Ribeirão Preto 14040-903 SP, Brazil;* orcid.org/0000-0002-4916-1505; Email: cristy@fcfrp.usp.br

Carolina H. Andrade − *Center for the Research and Advancement in Fragments and Molecular Targets (CRAFT), School of Pharmaceutical Sciences at Ribeirao Preto, University of São Paulo, Ribeirão Preto 14040-903 SP, Brazil; Laboratory for Molecular Modeling and Drug Design (LabMol), Faculty of Pharmacy, Universidade Federal de Goiás, Goiânia 74605-170 GO, Brazil; Center for Excellence in Artificial Intelligence (CEIA), Institute of Informatics, Universidade Federal de Goiás, Goiânia 74605-170 GO, Brazil;* orcid.org/0000-0003-0101-1492; Email: carolina@ufg.br

Flavio S. Emery − *Center for the Research and Advancement in Fragments and Molecular Targets (CRAFT), School of Pharmaceutical Sciences at Ribeirao Preto, University of São Paulo, Ribeirão Preto 14040-903 SP, Brazil; Laboratory of Heterocyclic and Medicinal Chemistry (QHeteM), Department of Pharmaceutical Sciences, School of Pharmaceutical Sciences at Ribeirao Preto, University of São*

https://doi.org/10.1021/acsmedchemlett.5c00237
ACS Med. Chem. Lett. 2026, 17, 99−108

Paulo, Ribeirão Preto 14040-903 SP, Brazil;
Email: flavioemery@usp.br

Authors

Bruna F. Godoi − *Center for the Research and Advancement in Fragments and Molecular Targets (CRAFT), School of Pharmaceutical Sciences at Ribeirao Preto, University of São Paulo, Ribeirão Preto 14040-903 SP, Brazil; Laboratory of Heterocyclic and Medicinal Chemistry (QHeteM), Department of Pharmaceutical Sciences, School of Pharmaceutical Sciences at Ribeirao Preto, University of São Paulo, Ribeirão Preto 14040-903 SP, Brazil*

Jéssica D. Bueno − *Center for the Research and Advancement in Fragments and Molecular Targets (CRAFT), School of Pharmaceutical Sciences at Ribeirao Preto, University of São Paulo, Ribeirão Preto 14040-903 SP, Brazil; Laboratory of Heterocyclic and Medicinal Chemistry (QHeteM), Department of Pharmaceutical Sciences, School of Pharmaceutical Sciences at Ribeirao Preto, University of São Paulo, Ribeirão Preto 14040-903 SP, Brazil*

Wemenes J. L. Silva − *Center for the Research and Advancement in Fragments and Molecular Targets (CRAFT), School of Pharmaceutical Sciences at Ribeirao Preto, University of São Paulo, Ribeirão Preto 14040-903 SP, Brazil; Laboratory for Molecular Modeling and Drug Design (LabMol), Faculty of Pharmacy, Universidade Federal de Goiás, Goiânia 74605-170 GO, Brazil; Center for Excellence in Artificial Intelligence (CEIA), Institute of Informatics, Universidade Federal de Goiás, Goiânia 74605-170 GO, Brazil*

Aline D. da Purificação − *Center for the Research and Advancement in Fragments and Molecular Targets (CRAFT), School of Pharmaceutical Sciences at Ribeirao Preto, University of São Paulo, Ribeirão Preto 14040-903 SP, Brazil; Protein Crystallography Laboratory, Department of Biomolecular Sciences, School of Pharmaceutical Sciences at Ribeirao Preto, University of São Paulo, Ribeirão Preto 14040-903 SP, Brazil*

Pedro I. P. Leite − *Center for the Research and Advancement in Fragments and Molecular Targets (CRAFT), School of Pharmaceutical Sciences at Ribeirao Preto, University of São Paulo, Ribeirão Preto 14040-903 SP, Brazil; Laboratory of Heterocyclic and Medicinal Chemistry (QHeteM), Department of Pharmaceutical Sciences, School of Pharmaceutical Sciences at Ribeirao Preto, University of São Paulo, Ribeirão Preto 14040-903 SP, Brazil*

Thiago dos Santos − *Center for the Research and Advancement in Fragments and Molecular Targets (CRAFT), School of Pharmaceutical Sciences at Ribeirao Preto, University of São Paulo, Ribeirão Preto 14040-903 SP, Brazil; Laboratory of Heterocyclic and Medicinal Chemistry (QHeteM), Department of Pharmaceutical Sciences, School of Pharmaceutical Sciences at Ribeirao Preto, University of São Paulo, Ribeirão Preto 14040-903 SP, Brazil*

Murillo Freitas − *Center for the Research and Advancement in Fragments and Molecular Targets (CRAFT), School of Pharmaceutical Sciences at Ribeirao Preto, University of São Paulo, Ribeirão Preto 14040-903 SP, Brazil; Laboratory for Molecular Modeling and Drug Design (LabMol), Faculty of Pharmacy, Universidade Federal de Goiás, Goiânia 74605-170 GO, Brazil*

Daniel G. Silva − *Center for the Research and Advancement in Fragments and Molecular Targets (CRAFT), School of Pharmaceutical Sciences at Ribeirao Preto, University of São Paulo, Ribeirão Preto 14040-903 SP, Brazil; Laboratory of Heterocyclic and Medicinal Chemistry (QHeteM), Department of Pharmaceutical Sciences, School of Pharmaceutical Sciences at Ribeirao Preto, University of São Paulo, Ribeirão Preto 14040-903 SP, Brazil;* Present Address: Universidade de São Paulo (USP) Faculdade de Ciências Farmacêuticas (FCF) Departamento de Tecnologia Bioquímico-Farmacêutica (FBT) Av. Prof. Lineu Prestes, 580 - Butantã, São Paulo - SP, 05508-000; orcid.org/0000-0001-8879-456X

Tais C. Silva − *Research Center on Neglected Diseases, Guarulhos University, Guarulhos 07023-070 SP, Brazl*

Josué de Moraes − *Research Center on Neglected Diseases, Guarulhos University, Guarulhos 07023-070 SP, Brazl; Research Center on Neglected Diseases, Scientific and Technological Institute, Brazil University, São Paulo 08230-030 SP, Brazil*

Caroline S. Freitas − *Laboratory of Immunopharmacology, Oswaldo Cruz Institute (IOC), Oswaldo Cruz Foundation (Fiocruz), Rio de Janeiro 21040-360 RJ, Brazil; National Institute for Science and Technology on Innovation in Diseases of Neglected Populations (INCT/IDPN), Center for Technological Development in Health (CDTS), Fiocruz, Rio de Janeiro 21040-900 RJ, Brazil*

Mayara Mattos − *Laboratory of Immunopharmacology, Oswaldo Cruz Institute (IOC), Oswaldo Cruz Foundation (Fiocruz), Rio de Janeiro 21040-360 RJ, Brazil; National Institute for Science and Technology on Innovation in Diseases of Neglected Populations (INCT/IDPN), Center for Technological Development in Health (CDTS), Fiocruz, Rio de Janeiro 21040-900 RJ, Brazil*

Thiago M. L. Souza − *Laboratory of Immunopharmacology, Oswaldo Cruz Institute (IOC), Oswaldo Cruz Foundation (Fiocruz), Rio de Janeiro 21040-360 RJ, Brazil; National Institute for Science and Technology on Innovation in Diseases of Neglected Populations (INCT/IDPN), Center for Technological Development in Health (CDTS), Fiocruz, Rio de Janeiro 21040-900 RJ, Brazil*

Bianca A. Martin − *Innovation Center in Nanostructured Systems and Topical Administration (NanoTop), School of Pharmaceutical Sciences at Ribeirao Preto, University of São Paulo, Ribeirão Preto 05508-060 SP, Brazil*

Renata F. V. Lopez − *Innovation Center in Nanostructured Systems and Topical Administration (NanoTop), School of Pharmaceutical Sciences at Ribeirao Preto, University of São Paulo, Ribeirão Preto 05508-060 SP, Brazil*

Complete contact information is available at: https://pubs.acs.org/10.1021/acsmedchemlett.5c00237

Author Contributions

B.F.G. synthesized the compounds, organized the synthetic and structure elucidation experimental data, discussed SAR, and wrote the manuscript. C.H.A. supervised and W.J.L.S. and M.F. provided computational and molecular modeling data. J.D.B., P.I.P.L., and T.S. also synthesized the compounds. D.G.S., B.A.M., and R.F.V.L. conducted water solubility assays. M.C.N supervised and A.D.P. performed biochemical and structural studies. T.M.L.S. supervised and C.S.F. and M.M. provided antiviral and cytotoxicity data against the Calu-3 cell line. T.C.S. and J.M. provided the cytotoxicity data against Vero and SH-SY5Y cells. F.S.E., C.H.A., and M.C.N.

https://doi.org/10.1021/acsmedchemlett.5c00237
ACS Med. Chem. Lett. 2026, 17, 99−108

coordinated, designed, and supervised the project and edited the manuscript. C.H.A. and M.C.N. acquired funding for this project. All authors critically reviewed and contributed to the final version of the paper. All authors have given approval to the final version of the manuscript.

Funding

The Article Processing Charge for the publication of this research was funded by the Coordenacao de Aperfeicoamento de Pessoal de Nivel Superior (CAPES), Brazil (ROR identifier: 00x0ma614). This work has been funded by CNPq BRICS STI COVID-19 (#441038/2020-4), FAPEG (#202010267000272), National Council for Scientific and Technological Development (CNPq grants 483659/2013-4, 4437502023-8, and 317060/2021-0), and São Paulo Research Foundation (FAPESP Grants #2020/06190-0, #2021/10084-3, #2021/13237-5, #2020/05369-6, #2023/07081-8, #2023/08418-6, #2023/11804-5, #2022/03521-0, #2024/08603-0, and #2013/08216-2). C.H.A., T.M.L.S., J.M., F.S.E., and M.C.N. are CNPq research fellows. T.S. was funded by NIH (R01 AI160379-01-NIH).

Notes

The authors declare no competing financial interest.

■ ACKNOWLEDGMENTS

The authors acknowledge the help with ESI-MS analyses from Dr. Jacqueline Nakau Mendonça Galiote Silva and Prof. Dr. Norberto Peporine Lopes (CEMMO/USP-RP).

■ ABBREVIATIONS

Calu-3, human lung epithelium; CC_{50}, cytotoxic concentration 50%; COVID-19, coronavirus disease 19; Da, Dalton; DCIP, 26-dichlorophenolindophenol; DCM, dichloromethane; DEMEM, Dulbecco's Modified Eagle Medium; DHO, dihydroorotate; DMSO, dimethyl sulfoxide; DNA, deoxyribonucleic acid; EC_{50}, half-maximal effective concentration; FBS, fetal bovine serum; FMN, flavin mononucleotide; GP, General Procedure; *Hs*DHODH, human dihydroorotate dehydrogenase; HEPES, (4-(2-hydroxyethyl)-1-piperazineethanesulfonic acid); HTS, high-throughput screening; IC_{50}, half-maximal inhibitory concentration; IR, infrared; LC-MS/MS, liquid chromatography−tandem mass spectrometry; MD, molecular dynamics; *m*, *meta*; MTT, thiazolyl blue tetrazolium bromide; MOI, multiplicity of infection; NADPH, nicotinamide adenine dinucleotide phosphate hydrogen; Ni-NTA, nickel−nitrilotriacetic acid; NMR, nuclear magnetic resonance; NPT, constant number of particles (N), system pressure (P), and temperature (T); NVT, constant number of particles (N), system volume (V), and temperature (T); *p*, *para*; PDB, Protein DataBank; PBS, phosphate-buffered saline; RDV, Remdesivir; RNA, ribonucleic acid; RMSD, root-mean-square deviation; SAR, structure−activity relationship; SARS-CoV-2, severe acute respiratory syndrome coronavirus 2; SD, standard deviation; SI, selectivity index; THF, tetrahydrofuran; TLC, thin-layer chromatography; UHPLC, ultra-high-performance liquid chromatography; UV, ultraviolet; Vero, African green monkey kidney; WHO, World Health Organization

■ REFERENCES

(1) Boschi, D.; Pippione, A. C.; Sainas, S.; Lolli, M. L. Dihydroorotate dehydrogenase inhibitors in anti-infective drug research. *Eur. J. Med. Chem.* **2019**, *183*, 111681.
(2) Reis, R. A. G.; Calil, F. A.; Feliciano, P. R.; Pinheiro, M. P.; Nonato, M. C. The dihydroorotate dehydrogenases: Past and present. *Arch. Biochem. Biophys.* **2017**, *632*, 175−191.
(3) Lipowska, J.; et al. Pyrimidine biosynthesis in pathogens - Structures and analysis of dihydroorotases from Yersinia pestis and Vibrio cholerae. *Int. J. Biol. Macromol.* **2019**, *136*, 1176−1187.
(4) Loffler, M.; Jockel, J.; Schuster, G. Dihydroorotat-ubiquinone oxidoreductase links mitochondria in the biosynthesis of pyrimidine nucleotides. *Mol. Cell. Biochem.* **1997**, *174*, 125.
(5) Cherwinski, H. M.; et al. The immunosuppressant leflunomide inhibits lymphocyte proliferation by inhibiting pyrimidine biosynthesis. *Journal of Pharmacology and Experimental Therapeutics* **1995**, *272*, 460.
(6) Kaur, H.; et al. Efficacy and safety of dihydroorotate dehydrogenase (DHODH) inhibitors "leflunomide" and "teriflunomide" in Covid-19: A narrative review. *Eur. J. Pharmacol.* **2021**, *906*, 174233.
(7) Miller, A. E. An Updated Review of teriflunomide's Use in Multiple Sclerosis. *Neurodegener Dis Manag* **2021**, *11*, 387−409.
(8) Coelho, A. R.; Oliveira, P. J. Dihydroorotate dehydrogenase inhibitors in SARS-CoV-2 infection. *European Journal of Clinical Investigation* **2020**, *50*, e13366.
(9) Kaur, H.; et al. Efficacy and safety of dihydroorotate dehydrogenase (DHODH) inhibitors "leflunomide" and "teriflunomide" in Covid-19: A narrative review. *Eur. J. Pharmacol.* **2021**, *906*, 174233.
(10) Zheng, Y.; et al. A Broad Antiviral Strategy: Inhibitors of Human DHODH Pave the Way for Host-Targeting Antivirals against Emerging and Re-Emerging Viruses. *Viruses* **2022**, *14*, 928.
(11) Smee, D. F.; Hurst, B. L.; Day, C. W. D282, a non-nucleoside inhibitor of influenza virus infection that interferes with de novo pyrimidine biosynthesis. *Antivir. Chem. Chemother.* **2012**, *22*, 263.
(12) Gong, M.; et al. Novel quinolone derivatives targeting human dihydroorotate dehydrogenase suppress Ebola virus infection in vitro. *Antiviral Res.* **2021**, *194*, 105161.
(13) Zhang, L.; et al. Recent advances of human dihydroorotate dehydrogenase inhibitors for cancer therapy: Current development and future perspectives. *Eur. J. Med. Chem.* **2022**, *232*, 114176.
(14) Khairy, A.; Hammoda, H. M.; Celik, I.; Zaatout, H. H.; Ibrahim, R. S. Discovery of potential natural dihydroorotate dehydrogenase inhibitors and their synergism with Brequinar via integrated molecular docking, dynamic simulations and in vitro approach. *Sci. Rep.* **2022**, *12*, 19037.
(15) Luban, J.; et al. The DHODH inhibitor PTC299 arrests SARS-CoV-2 replication and suppresses induction of inflammatory cytokines. *Virus Res.* **2021**, *292*, 198246.
(16) PTC Therapeutics. A Study to Evaluate Efficacy and Safety of PTC299 (Emvododstat) in Hospitalized Participants With Coronavirus (COVID-19) (FITE19), June 26, 2023. https://clinicaltrials.gov/study/NCT04439071?intr=emvododstat&k=2.
(17) Luganini, A.; Boschi, D.; Lolli, M. L.; Gribaudo, G. DHODH inhibitors: What will it take to get them into the clinic as antivirals? *Antiviral Res.* **2025**, *236*, 106099.
(18) Schrell, L.; et al. Inhibitors of dihydroorotate dehydrogenase synergize with the broad antiviral activity of 4′-fluorouridine. *Antiviral Res.* **2025**, *233*, 106046.
(19) Purificação, A. D.; et al. Unveiling the Antiviral Capabilities of Targeting Human Dihydroorotate Dehydrogenase against SARS-CoV-2. *ACS Omega* **2024**, *9*, 11418−11430.
(20) Baell, J. B.; Nissink, J. W. M. Seven Year Itch: Pan-Assay Interference Compounds (PAINS) in 2017 - Utility and Limitations. *ACS Chem. Biol.* **2018**, *13*, 36−44.
(21) Gilberg, E.; Stumpfe, D.; Bajorath, J. Activity profiles of analog series containing pan assay interference compounds. *RSC Adv.* **2017**, *7*, 35638−35647.
(22) Cho, W.; et al. Synthesis of New Bis(amidine)-Cobalt Catalysts and Their Application to Styrene Polymerization. *Organometallics* **2014**, *33*, 1617−1622.

https://doi.org/10.1021/acsmedchemlett.5c00237
ACS Med. Chem. Lett. 2026, 17, 99−108

(23) Yang, Y.; et al. An Efficient Synthesis of Quinoxalinone Derivatives as Potent Inhibitors of Aldose Reductase. *ChemMedChem* **2012**, *7*, 823−835.
(24) Christopher Bi, F.; Aspnes, G. E.; Guzman-Perez, A.; Walker, D. P. Novel syntheses of 3-anilino-pyrazin-2(1H)-ones and 3-anilino-quinoxalin-2-(1H)-ones via microwave-mediated Smiles rearrangement. *Tetrahedron Lett.* **2008**, *49*, 1832−1835.
(25) Scribner, A.; et al. Synthesis and biological activity of anticoccidial agents: 5,6-Diarylimidazo[2,1-b][1,3]thiazoles. *Bioorg. Med. Chem. Lett.* **2008**, *18*, 5263.
(26) Zhou, Z.; et al. Design, synthesis and evaluation of anti-proliferative activity of 2-aryl-4-aminoquinazoline derivatives as EGFR inhibitors. *Bioorg Chem.* **2021**, *112*, 104848.
(27) Daikopoulou, V.; et al. Targeting SARS-COV-2 polymerase with new nucleoside analogues. *Molecules* **2021**, *26*, 3960.
(28) Deruiter, J.; Brubaker, A. N.; Millen, J.; Riley, T. N. Design and Synthesis of 2-(Arylamino)-4(3ff)-Quinazolinones as Novel Inhibitors of Rat Lens Aldose Reductase. *J. Med. Chem.* **1986**, *29*, 627.
(29) Zuo, Z. Erratum: Bifunctional Naphtho[2,3- d][1,2,3]triazole-4,9-dione Compounds Exhibit Antitumor Effects in Vitro and in Vivo by Inhibiting Dihydroorotate Dehydrogenase and Inducing Reactive Oxygen Species Production (Journal of Medicinal Chemistry (2020) 63:14 (7633−7652) DOI: 10.1021/acs.jmedchem.0c00512). *J. Med. Chem.* **2020**, *63*, 10532.
(30) Baumgartner, R.; et al. Dual Binding Mode of a Novel Series of DHODH Inhibitors. *J. Med. Chem.* **2006**, *49*, 1239−1247.
(31) Batt, D. G.; et al. Immunosuppressive structure-activity relationships of Brequinar and related cinchoninic acid derivatives. *Bioorg. Med. Chem. Lett.* **1995**, *5*, 1549−1554.
(32) Wei, W.; Cherukupalli, S.; Jing, L.; Liu, X.; Zhan, P. Fsp3: A new parameter for drug-likeness. *Drug Discov. Today* **2020**, *25*, 1839−1845.

https://doi.org/10.1021/acsmedchemlett.5c00237
ACS Med. Chem. Lett. 2026, 17, 99−108